EPTT 2024
Escola de Primavera de Transição e Turbulência

ABCM
Associação Brasileira de Engenharia e Ciências Mecânicas

INVESTIGATION OF SPANWISE PERIODIC TRANSITIONAL AIRFOIL FLOWS USING THE LATTICE-BOLTZMANN METHOD

Cayan A. Dantas*
Bernardo Luiz R. Ribeiro†
William R. Wolf‡
University of Campinas, Campinas, SP, Brazil, 13083-860
c253092@dac.unicamp.br*
beluiz@unicamp.br†
wolf@fem.unicamp.br‡

Abstract. *The present study evaluates the capability of a lattice-Boltzmann high-fidelity simulation tool to resolve transitional flows with intermittent events. Here, the lattice-Boltzmann method (LBM) is employed to investigate the spanwise-periodic flow over a NACA0012 airfoil at an angle of attack of* $\boldsymbol{\alpha = 3°}$*, freestream Mach number of* $\boldsymbol{M_\infty = 0.3}$*, and Reynolds number* $\boldsymbol{Re = 5 \times 10^4}$*. For this particular case, a laminar separation bubble forms on the airfoil suction side, being responsible for a complex dynamics including the shedding of coherent structures that generate trailing-edge tonal noise. A grid convergence study is performed for the LBM and results are validated against large eddy simulations (LES) of the Navier-Stokes equations. Good comparisons are observed between the LBM and LES results in terms of time-averaged flow fields. Similar separation and reattachment locations are found for the suction side laminar separation bubble (LSB). An analysis in terms of the vortex dynamics is also presented, and different patterns of vortex shedding from the LSB are found, in agreement with LES results. In summary, the LBM approach is able to represent similar flow physics compared to the Navier-Stokes equations, but with around* 10% *of the computational cost of the LES.*

Keywords: *Lattice-Boltzmann, transitional flow, laminar separation bubble*

1. INTRODUCTION

The analysis of noise generation mechanisms in airfoils has been key to the development of quieter air vehicles. For this purpose, flows at various Reynolds numbers including laminar, transitional, and turbulent regimes, besides different airfoils and angles of attack have been extensively investigated in the literature (Paterson *et al.*, 1972; Arbey and Bataille, 1983; Brooks *et al.*, 1989; Moreau *et al.*, 2011; Wolf *et al.*, 2012; Pröbsting *et al.*, 2015; Ricciardi and Wolf, 2022; Sano *et al.*, 2023). In this work, the same configuration from Ricciardi *et al.* (2022) is investigated, i.e., we perform 3D numerical simulations of a spanwise periodic flow over a NACA0012 airfoil at Reynolds number $Re = 5 \times 10^4$, freestream Mach number of $M_\infty = 0.3$, and angle of attack $\alpha = 3°$.

Depending on the Reynolds number, different mechanisms drive the acoustic noise generation. At low to moderate values ($Re < 10^5$), the flow events over the foil's suction side dominate over the pressure side, whereas at high values, the opposite becomes true (Pröbsting *et al.*, 2015; Ricciardi and Wolf, 2022). A major feature of low Reynolds number flows consists in the formation of a laminar separation bubble (LSB) on the airfoil suction side. This bubble is shown to have an intermittent behavior which modulates the shedding of coherent structures advected towards the trailing edge (TE) (Ricciardi *et al.*, 2020). Pröbsting and Yarusevych (2015) showed that a NACA0012 airfoil at Reynolds numbers 0.65 x $10^5 \leq Re \leq 4.5$ x 10^5 and $\alpha = 2°$ presents intermittent laminar–turbulent transition that affects the convection of coherent structures from the LSB over the suction side towards the TE. In this case, scattering of these spanwise-coherent structures is a major mechanism for airfoil noise generation.

More recently, Ricciardi *et al.* (2022) showed through linear stability analysis that the vortex merging and bursting over the foil's suction side depends on the constructive phase interference between the unstable frequencies observed in the linear eigenspectrum. When these are in phase, it is likely that a successful event of vortex merging occurs, otherwise vortex bursting might happen and finer turbulence structures forms. These authors also showed that the noise spectrum depicts a main tone with multiple equidistant secondary tones, in agreement with previous studies (Paterson *et al.*, 1972; Arbey and Bataille, 1983). The acoustic disturbances emitted at the TE were also shown to close an acoustic feedback

loop when reaching the most receptive region near the leading edge.

While the dynamics of the LSB has been analyzed at different flow conditions including various Reynolds numbers and angles of attack, the spanwise effects of the vortex merging and bursting processes are still considered to be a complex phenomena as noted by Michelis *et al.* (2018). Ricciardi *et al.* (2022) showed that, using periodic boundary conditions, there is a strong spanwise vortex coherence before the transition to turbulence in a simulation of an extruded airfoil with span equal to 40% of the chord length. The study of a transitional airfoil flow over a finite wing is presented in the second part of this work, and it is shown that the wing tip vortices considerably impact the LSB formation and the ejection of coherent structures through the TE (Ribeiro *et al.*, 2024).

The objective of this paper is to perform an assessment of the lattice-Boltzmann method (LBM) in resolving a transitional airfoil flow with spanwise periodic boundary conditions. This analysis is performed through 3D numerical simulations which are conducted using a high-fidelity LBM-CFD tool. The simulations are run in direct numerical simulation (DNS) mode, i.e., without subgrid scale or wall models which are available in the present LBM solver. Due to its simpler partial differential equation system compared to the traditional Navier-Stokes solvers, the LBM offers advantages in terms of simulation time and scalability (Moreau *et al.*, 2011). Results are compared to available data from Ricciardi *et al.* (2022) and are presented for different mesh configurations in terms of mean values. Finally, the dynamics of coherent structures is evaluated for the present flows.

2. METHODOLOGY

2.1 Numerical Simulations

2.1.1 Lattice-Boltzmann solver

Numerical simulations are conducted using the commercial code SIMULIA PowerFLOW 6-2022, a high-fidelity LBM-based software. The LBM resolves fluid flows at the mesoscopic scale in a statistical sense, having origin in the lattice gas models (Krüger *et al.*, 2017). While these models track the behavior of particles at a microscopic scale, the LBM instead tracks the advection and collision of fluid particles using discrete distribution functions $f_i(\boldsymbol{x}, t)$, often called particle populations (Teruna *et al.*, 2020). The term f_i represents the density of particles travelling with velocity $\boldsymbol{c} = (c_x, c_y, c_z)$ from the position $\boldsymbol{x} = (x, y, z)$ at a time t in the direction i. The velocity is chosen so that particles travel one cell per timestep, effectively making the Courant–Friedrichs–Lewy (CFL) number for f_i equal to one Ribeiro *et al.* (2016). The LBM equation (Chen *et al.*, 1997) is written as

$$f_i(\boldsymbol{x} + \boldsymbol{c}_i\Delta t, t + \Delta t) - f_i(\boldsymbol{x}, t) = \Omega_i(\boldsymbol{x}, t)\,, \tag{1}$$

where Ω_i represents the collision operator and Δt is the timestep. The left-hand side of Eq. (1) represents particles moving with velocity $\boldsymbol{c}$ in the i-th direction to a neighbouring point $\boldsymbol{x} + \boldsymbol{c}_i\Delta t$ at the next timestep $t + \Delta t$. On the right-hand side, particle collisions are modeled by redistributing them among f_i at each site. In PowerFLOW, the collision term is modeled using the approximation described by Bhatnagar *et al.* (1954) as

$$\Omega_i(\boldsymbol{x}, t) = -\frac{\Delta t}{\tau}[f_i(\boldsymbol{x}, t) - f_i^{eq}(\boldsymbol{x}, t)]\,, \tag{2}$$

where τ is the relaxation time, which is related to the non-dimensional fluid viscosity ν through the relation $\nu = c_s^2(\tau - \Delta t/2)$ (Ribeiro *et al.*, 2018). Here, c_s is the non-dimensional speed of sound, and the term f_i^{eq} is the equilibrium Maxwell-Boltzmann distribution function, which is approximated by a second-order expansion (Chen *et al.*, 1992) as

$$f_i^{eq} = w_i\rho\left(1 + \frac{\boldsymbol{c}_i \cdot \boldsymbol{u}}{c_s^2} + \frac{(\boldsymbol{c}_i \cdot \boldsymbol{u})^2}{2c_s^4} - \frac{\boldsymbol{u} \cdot \boldsymbol{u}}{2c_s^2}\right)\,, \tag{3}$$

where w_i represents weighting coefficients which depend on the direction being calculated, while ρ is the fluid density and $\boldsymbol{u}$ is the fluid velocity. Together with a corresponding set of w_i, $\boldsymbol{c}_i$ forms velocity sets usually denoted by DdQq, where d is the number of spatial dimensions of the velocity set, and q represents the number of discrete velocity directions. In PowerFLOW, the D3Q19 velocity set is used for three-dimensional flows (Himeno *et al.*, 2021).

The phenomenon of transition to turbulence requires a level of spatial and temporal resolution that is compatible with direct numerical simulation (DNS) or wall-resolved large eddy simulation (LES). The turbulence modeling capability of PowerFLOW (Chen *et al.*, 2003), which enables a numerical procedure called very large eddy simulation (VLES), has not been shown to capture laminar-turbulence transition yet. Therefore, in the present work we perform simulations in the DNS mode, i.e., we do not employ subgrid or wall models available in the solver.

The link between Eq. (1) and the Navier-Stokes (NS) equations can be determined using the Chapman-Enskog analysis (Chapman *et al.*, 1990). Once f_i is known, macroscopic flow variables, such as ρ and $\boldsymbol{u}$ are obtained by taking the zeroth-

and first-order moments of f_i (Souza *et al.*, 2019), respectively:

$$\rho(\boldsymbol{x},t) = \sum_{i=0}^{q-1} f_i(\boldsymbol{x},t)\ , \tag{4}$$

and

$$\rho(\boldsymbol{x},t)\boldsymbol{u}(\boldsymbol{x},t) = \sum_{i=0}^{q-1} \boldsymbol{c}_i f_i(\boldsymbol{x},t)\ . \tag{5}$$

The LBM is solved on a lattice composed of cubic volumetric elements called voxels. The simulation domain can be subdivided into several regions where different voxel resolutions are applied (Teruna *et al.*, 2021), such that the resolution between two adjacent regions varies by a factor of 2. Solid boundaries are discretized using computational surface elements (surfels) that are generated at locations where the voxels intersect solid surfaces (facets) (Chen *et al.*, 1998). The process of generating voxels and surfels is fully automated. The boundary condition at a solid wall is computed by applying appropriate particle interactions in the collision term of the LBM. PowerFLOW results are transient and time accurate, where the time advancement is performed by an explicit scheme which allows for efficient and highly-scalable simulations.

2.1.2 Navier-Stokes solver

The Navier-Stokes simulation results utilized for comparison in this manuscript are extracted from the work by Ricciardi *et al.* (2022). A wall-resolved large eddy simulation (LES) was performed to solve the compressible Navier–Stokes equations in general curvilinear coordinates in order to study secondary tones generated by a NACA0012 airfoil at angle of attack of $\alpha = 3^o$ with freestream Mach number of $M_\infty = 0.3$ and Reynolds number of $Re = 5 \times 10^4$. The spatial discretization of the governing equations employed a sixth-order accurate compact scheme for derivatives and interpolations on a staggered grid. The time integration was carried out by a hybrid implicit–explicit method, where an implicit second-order scheme is applied in the near-wall region, while the outer region employs a third-order Runge-Kutta scheme. Away from the wall, a sixth-order compact filter is applied. No-slip adiabatic wall boundary conditions are enforced along the airfoil surface and characteristic plus sponge boundary conditions are applied in the far-field locations to minimise wave reflections. Periodic boundary conditions were used in the spanwise direction.

2.2 Flow configuration and mesh details

The flow over a NACA0012 airfoil is investigated for a Reynolds number of $Re = 5 \times 10^4$, freestream Mach number of $M_\infty = 0.3$ and angle of attack $\alpha = 3°$. The TE is modified as shown in Fig. 1. The airfoil with chord length c is located at the center of the computational domain. The airfoil span is 40% of the airfoil chord and periodic boundary conditions are employed to compare results with Ricciardi *et al.* (2022). Outlet boundary conditions are applied on the right, top and bottom planes of the computational domain, while an inlet is defined in the left plane which is the surface closest to the leading edge and perpendicular to the foil chord. The farfield boundary conditions are located 30 chords away from the center of the profile on each direction. A no-slip boundary condition is specified at the airfoil surface and no turbulence modelling is used in the present study in order to assess the capability of the LBM to capture the laminar to turbulent transition of the boundary layer.

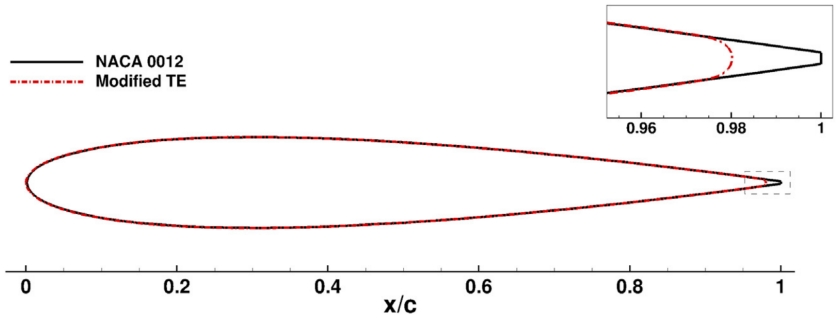

Figure 1: Modified NACA0012 TE profile. Figure taken from Ricciardi *et al.* (2022).

A mesh refinement analysis is performed and three meshes with different refinements are utilized. All meshes are composed of 11 variable resolution (VR) regions that control the voxel size from the foil surface to the outer domain. The difference across meshes is only related to the number of voxels along the airfoil chord. The coarse, baseline and fine meshes have approximately 4000, 5120, and 6400 voxels around the foil. The three finest VR regions are applied as

an offset of the NACA0012 profile (see Figs. 2a, 2c, and 2e), while the other 8 VRs are hexahedral boxes enclosing it, where a domain subset is shown in Figs. 2b, 2d, and 2f. The height of each offset is equivalent to 20 voxels in all meshes. The finest voxel size is 0.0246%, 0.0195%, and 0.0156% of the chord from the coarsest to the finest resolution. The mesh is constructed so that the boundary layer fits inside the two finest regions and there is a total of 450, 512, and 652 million voxels in the domain from the coarse to the fine grid refinement. To obtain convergence of the flow statistics, the simulations are performed for 80 convective time units $tc/U_\infty = 80$ using approximately 700 AMD EPYC 7443 cores for around 1.7×10^5 CPU hours. To remove the transient region before reaching a quasi-steady regime, the first $tc/U_\infty = 30$ time units are removed from the analysis.

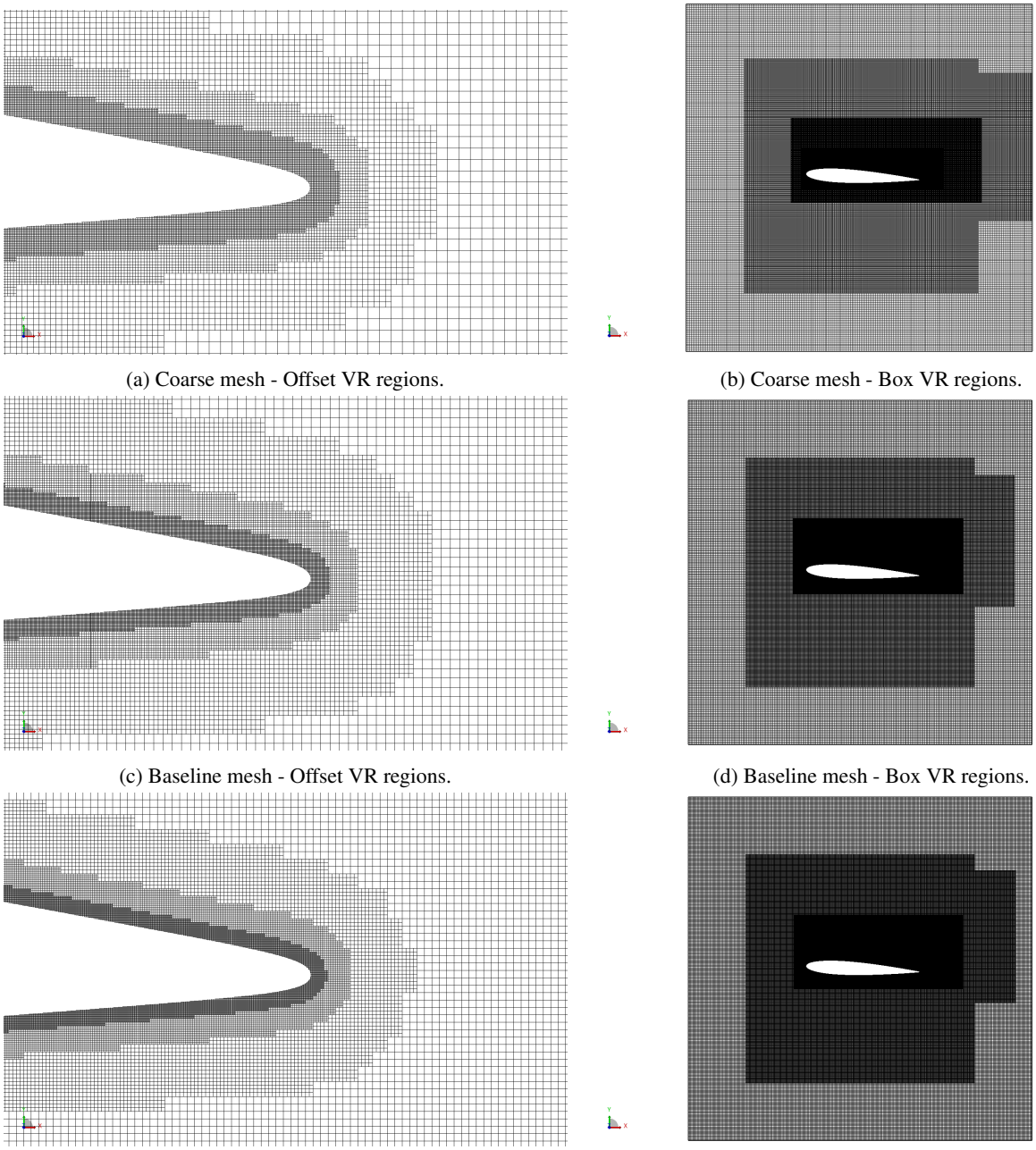

(a) Coarse mesh - Offset VR regions.

(b) Coarse mesh - Box VR regions.

(c) Baseline mesh - Offset VR regions.

(d) Baseline mesh - Box VR regions.

(e) Fine mesh - Offset VR regions.

(f) Fine mesh - Box VR regions.

Figure 2: Mesh details for three different refinements. Left column illustrates the offset regions while the right column displays the box VR regions.

3. RESULTS

Results are presented for the LBM and NS solvers, being divided in two parts, namely the mean flow and vortex dynamics analyses.

3.1 Mean flow analysis

First, we analyze the mean flow LBM solutions in terms of the LSB size and location. For this, the time- and spanwise-averaged streamwise velocity flow field is computed and compared against the Navier-Stokes simulation from Ricciardi *et al.* (2022), as displayed in Fig. 3. The magenta dashed lines in both the LBM and NS simulations depict the reversed flow boundaries which include a wide separation bubble on the suction side, besides a small LSB on the pressure side, near the trailing edge. As can be seen from the figure, the mean velocity fields are in excellent agreement for all simulations and all LBM mesh resolutions.

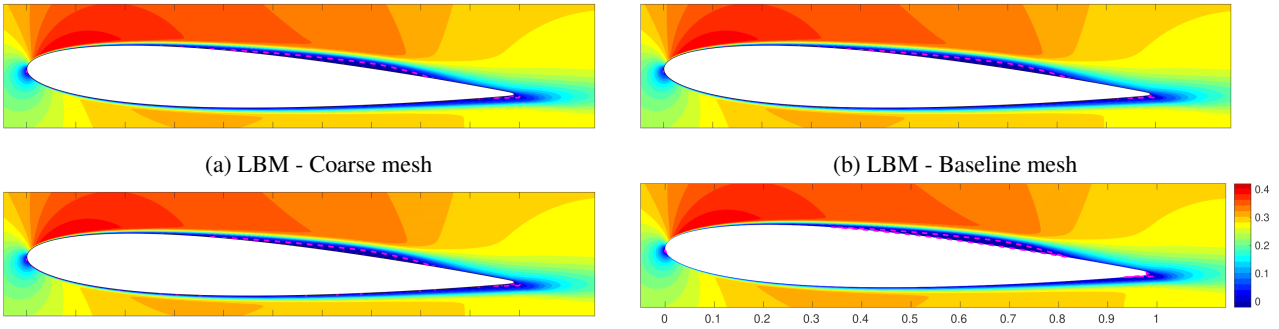

(a) LBM - Coarse mesh (b) LBM - Baseline mesh

(c) LBM - Fine mesh (d) NS

Figure 3: Contours of mean streamwise velocity $\overline{u}$ normalized by the freestream speed of sound. The magenta dashed lines highlight the reversed flow boundaries which display a separation bubble on the suction side in addition to a small bubble on the pressure side, near the trailing edge. Figure 3d is generated with data from Ricciardi *et al.* (2022).

To extract the location with the highest disturbances of the flow over the airfoil, the root-mean-square (RMS) of the pressure fluctuation (p') and turbulent kinetic energy (k) are computed. Figure 4 shows contours of pressure fluctuations for all LBM meshes and the NS solution. The latter is computed for a small grid domain which includes only the implicit grid region of the LES. An excellent agreement between the LBM and NS methodologies is observed both in terms of magnitude of the pressure RMS and the location of maximum disturbances, which correspond to the LSB reattachment region on the suction side of the airfoil. This metric also shows the mesh independence since for all LBM cases, the location of highest disturbance is comparable.

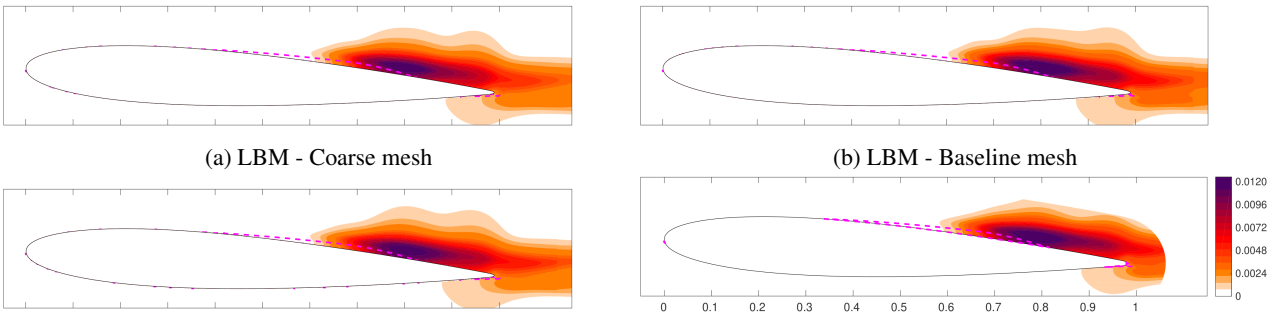

(a) LBM - Coarse mesh (b) LBM - Baseline mesh

(c) LBM - Fine mesh (d) NS

Figure 4: Contours of root-mean-square of pressure fluctuation p' normalized by the freestream density and speed of sound. The magenta dashed lines highlight the reversed flow boundaries. Figure 4d is computed with data from Ricciardi *et al.* (2022).

Similarly, Fig. 5 highlights the LBM mesh independence results in terms of turbulent kinetic energy k. For this quantity, negligible differences are observed when compared with the NS results. The overall spatial distribution of k, including its values, are similar among all simulations. However, some residual values appear for the fine mesh of the LBM solution along the outer region of the boundary layer. Further analysis will be conducted to investigate the origin of these fluctuations. Comparing Figs. 4 and 5, both depict highest values close to the reattachment region on the suction side, with k values more spread across near the trailing edge, differently from the more localized RMS values of p'.

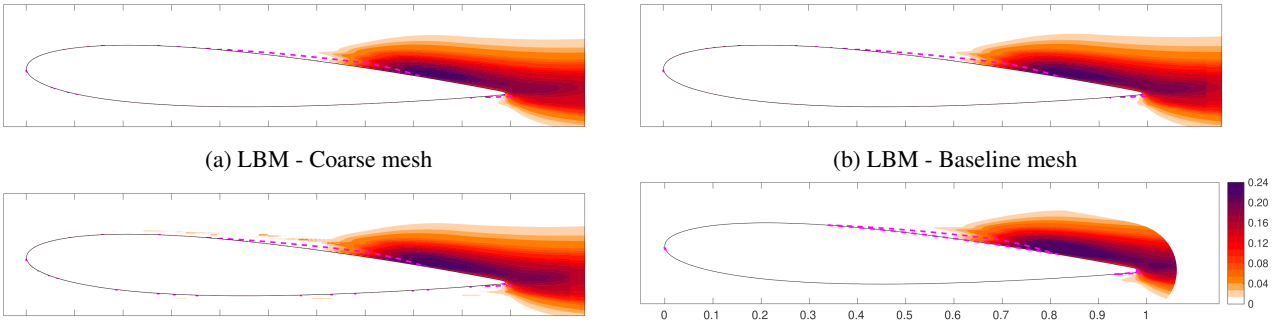

(a) LBM - Coarse mesh (b) LBM - Baseline mesh

(c) LBM - Fine mesh (d) NS

Figure 5: Contours of turbulent kinetic energy k normalized by the freestream velocity. The magenta dashed lines highlight the reversed flow boundaries. Data from Fig. 5d is taken using data from Ricciardi *et al.* (2022).

3.2 Vortex dynamics analysis

In this section, we investigate the vortex dynamics of the present transient flow. Although the mean flow fields and the boundary layer analysis provide a comparison between the LBM and NS methodologies, the study of the vortex dynamics reveals further details of the transient flow features. Ricciardi *et al.* (2022) show that vortex pairing and merging may lead to coherent structures transported through the trailing edge. In some cases, the pairing may not be successful and lead to bursting of fine turbulent scales. The first set of results shown in Fig. 6 compare snapshots with isosurfaces of Q-criterion colored by the streamwise velocity u. While the left plot shows turbulent structures at the trailing edge, the right one shows the transport of spanwise coherent vortices shed by the bubble. Hence, the LBM is able to detect the intermittent laminar–turbulent transition that affects the convection of coherent structures from the laminar separation bubble over the suction side towards the TE.

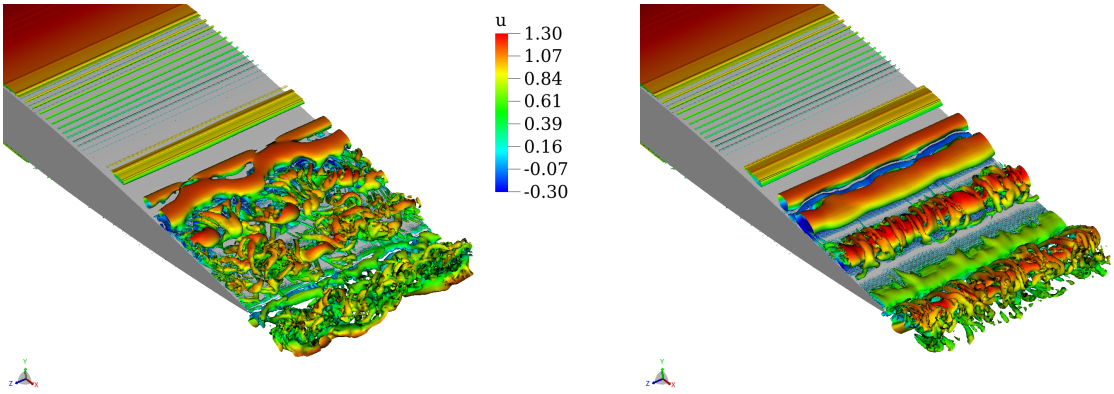

(a) LBM: turbulent structures (b) LBM: spanwise coherence

Figure 6: Instantaneous isosurfaces of Q-criterion colored by the streamwise velocity u. Two regimes are shown where (a) shows vortices with lower coherence, generating smaller-scale turbulent eddies, and (b) displays spanwise-correlated structures shed from the bubble.

4. CONCLUSIONS

We perform an assessment of the LBM for solving a transitional airfoil flow. Results from the LBM are compared to those from Ricciardi *et al.* (2022), obtained for a wall-resolved LES that solves the Navier-Stokes (NS) equations. The numerical simulations are performed for a NACA0012 airfoil with Reynolds number $Re = 5 \times 10^4$, freestream Mach number of $M_\infty = 0.3$, and angle of attack $\alpha = 3°$. The objective of this work is to validate the LBM results for a spanwise-periodic flow. A grid refinement study is performed for the LBM and results are validated in terms of mean flow quantities and RMS of metrics in the analysis of the boundary layer development. Good agreement is found for time-averaged flow fields computed by the LBM and NS approaches. An investigation in terms of the vortex dynamics on the airfoil suction side is also presented.

5. ACKNOWLEDGEMENTS

The authors thank CENAPAD-SP (Project 551 - Cluster Lovelace) for providing the computational resources used in this study. We acknowledge Fundação de Amparo à Pesquisa do Estado de São Paulo (FAPESP) for supporting the present work under research grants No. 2013/08293-7, 2021/06448-0 and 2023/08768-7. We also acknowledge a scholarship to the first author funded by Coordenação de Aperfeiçoamento de Pessoal de Nível Superior, CAPES, under grant 88887.825328/2023-00.

6. REFERENCES

Arbey, H. and Bataille, J., 1983. "Noise generated by airfoil profiles placed in a uniform laminar flow". *Journal of Fluid Mechanics*, Vol. 134, pp. 33–47. ISSN 1469-7645. doi:10.1017/S0022112083003201.

Bhatnagar, P.L., Gross, E.P. and Krook, M., 1954. "A model for collision processes in gases. i. small amplitude processes in charged and neutral one-component systems". *Physical Review*, Vol. 94, pp. 511–525. doi:10.1103/PhysRev.94.511.

Brooks, T.F., Pope, D.S. and Marcolini, M.A., 1989. "Airfoil self-noise and prediction". Technical report, NASA.

Chapman, S., Cowling, T.G. and Park, D., 1990. "The mathematical theory of non-uniform gases". Cambridge University Press. doi:https://doi.org/10.2307/3607024.

Chen, H., Chen, S. and Matthaeus, W.H., 1992. "Recovery of the navier-stokes equations using a lattice-gas boltzmann method". *Physical Review*, Vol. 45, pp. R5339–R5342. doi:10.1103/PhysRevA.45.R5339.

Chen, H., Kandasamy, S., Orszag, S., Shock, R., Succi, S. and Yakhot, V., 2003. "Extended boltzmann kinetic equation for turbulent flows". *Science*, Vol. 301, pp. 633–636. doi:https://doi.org/10.1126/science.1085048.

Chen, H., Teixeira, C. and Molvig, K., 1997. "Digital physics approach to computational fluid dynamics: Some basic theoretical features". *International Journal of Modern Physics C*, Vol. 8, p. 675–684. doi:10.1142/s0129183197000576.

Chen, H., Teixeira, C. and Molvig, K., 1998. "Realization of fluid boundary conditions via discrete boltzmann dynamics". *International Journal of Modern Physics C*, Vol. 9, pp. 1281–1292. doi:10.1142/s0129183198001151.

Himeno, F.H., Souza, D.S., Amaral, F.R., Rodríguez, D. and Medeiros, M.A., 2021. "Spod analysis of noise-generating rossiter modes in a slat with and without a bulb seal". *Journal of Fluid Mechanics*, Vol. 915, No. A67. doi:10.1017/jfm.2021.93.

Krüger, T., Kusumaatmaja, H., Kuzmin, A., Shardt, O., Silva, G. and Viggen, E.M., 2017. *The Lattice-Boltzmann Method*, Vol. 10. Springer International Publishing. doi:https://doi.org/10.1007/978-3-319-44649-3.

Michelis, T., Yarusevych, S. and Kotsonis, M., 2018. "On the origin of spanwise vortex deformations in laminar separation bubbles". *Journal of Fluid Mechanics*, Vol. 841, pp. 81–108. ISSN 0022-1120, 1469-7645. doi:10.1017/jfm.2018.91.

Moreau, S., Sanjosé, M., Perot, F. and Kim, M.S., 2011. "Direct self-noise simulation of the installed Controlled Diffusion airfoil". In *17th AIAA/CEAS Aeroacoustics Conference (32nd AIAA Aeroacoustics Conference)*. American Institute of Aeronautics and Astronautics, Portland, Oregon. ISBN 978-1-60086-943-3. doi:10.2514/6.2011-2716.

Paterson, R.W., Vogt, P.G., Fink, M.R. and Munch, C.L., 1972. "Vortex noise of isolated airfoils". *Journal of Aircraft*, Vol. 10, pp. 296–302. doi:DOI:10.2514/3.60229.

Pröbsting, S., Scarano, F. and Morris, S.C., 2015. "Regimes of tonal noise on an airfoil at moderate Reynolds number". *Journal of Fluid Mechanics*, Vol. 780, pp. 407–438. ISSN 0022-1120, 1469-7645. doi:10.1017/jfm.2015.475.

Pröbsting, S. and Yarusevych, S., 2015. "Laminar separation bubble development on an airfoil emitting tonal noise". *Journal of Fluid Mechanics*, Vol. 780, pp. 167–191. ISSN 0022-1120, 1469-7645. doi:10.1017/jfm.2015.427.

Ribeiro, A., Fares, E. and Choudhari, M., 2018. "Dns of laminar to turbulent transition on naca 0012 airfoil with sand grain roughness". Technical report, NASA.

Ribeiro, A.F.P., Casalino, D., Fares, E. and Choudhari, M., 2016. "Direct numerical simulation of an airfoil with sand grain roughness on the leading edge". Technical report, NASA.

Ribeiro, B.L.R., Dantas, C.A. and Wolf, W.R., 2024. "Assessment of transitional airfoil flows through the lattice-boltzmann method part ii: Finite wing effects". In *AIAA Aviation 2024 Forum*. American Institute of Aeronautics and Astronautics, Las Vegas, Nevada.

Ricciardi, T.R., Arias-Ramirez, W. and Wolf, W.R., 2020. "On secondary tones arising in trailing-edge noise at moderate Reynolds numbers". *Eur. J. Mech. B*, Vol. 79, pp. 54–66. ISSN 0997-7546. doi:10.1016/j.euromechflu.2019.08.015.

Ricciardi, T.R. and Wolf, W.R., 2022. "Switch of tonal noise generation mechanisms in airfoil transitional flows". *Physical Review Fluids*, Vol. 7, No. 8, p. 084701. ISSN 2469-990X. doi:10.1103/PhysRevFluids.7.084701.

Ricciardi, T.R., Wolf, W.R. and Taira, K., 2022. "Transition, intermittency and phase interference effects in airfoil secondary tones and acoustic feedback loop". *Journal of Fluid Mechanics*, Vol. 937, p. A23. ISSN 0022-1120, 1469-7645. doi:10.1017/jfm.2022.129.

Sano, A., Cavalieri, A.V., da Silva, A.F. and Wolf, W.R., 2023. "On the emergence of secondary tones in airfoil noise". *Journal of Fluid Mechanics*, Vol. 966, p. A8. doi:10.1017/jfm.2023.442.

Souza, D.S., Rodríguez, D., Himeno, F.H.T. and Medeiros, M.A.F., 2019. "Dynamics of the large-scale structures and associated noise emission in airfoil slats". *Journal of Fluid Mechanics*, Vol. 875, p. 1004–1034. doi:

10.1017/jfm.2019.496.

Teruna, C., Avallone, F., Ragni, D., Rubio-Carpio, A. and Casalino, D., 2021. "Numerical analysis of a 3-d printed porous trailing edge for broadband noise reduction". *Journal of Fluid Mechanics*, Vol. 926, No. A17. doi: 10.1017/jfm.2021.704.

Teruna, C., Manegar, F., Avallone, F., Ragni, D., Casalino, D. and Carolus, T., 2020. "Noise reduction mechanisms of an open-cell metal-foam trailing edge". *Journal of Fluid Mechanics*, Vol. 898, No. A18. doi:10.1017/jfm.2020.363.

Wolf, W.R., Azevedo, J.L.F. and Lele, S.K., 2012. "Convective effects and the role of quadrupole sources for aerofoil aeroacoustics". *Journal of Fluid Mechanics*, Vol. 708, pp. 502–538. ISSN 0022-1120, 1469-7645. doi: 10.1017/jfm.2012.327.

7. RESPONSIBILITY NOTICE

The authors are the only responsible for the printed material included in this paper.